Osaka University Knowledge Archive : OUKA

https://ir.library.osaka-u.ac.jp/

Osaka University

P H Y S I C A L   R E V I E W   L E T T E R S

Surface Acceleration of Fast Electrons with Relativistic Self-Focusing in Preformed Plasma

H. Habara,[1,2] K. Adumi,[1] T. Yabuuchi,[1] T. Nakamura,[2] Z. L. Chen,[1] M. Kashihara,[1] R. Kodama,[1,2] K. Kondo,[1,2]
G. R. Kumar,[1,*] L. A. Lei,[1] T. Matsuoka,[1,†] K. Mima,[2] and K. A. Tanaka[1,2]

[1]*Graduate School of Engineering, Osaka University, 2-1, Yamada-oka, Suita, Osaka 565-0871, Japan*
[2]*Institute of Laser Engineering, Osaka University, 2-6, Yamada-oka, Suita, Osaka 565-0871, Japan*
(Received 9 March 2006; published 1 September 2006)

We report an observation of surface acceleration of fast electrons in intense laser-plasma interactions. When a preformed plasma is presented in front of a solid target with a higher laser intensity, the emission direction of fast electrons is changed to the target surface direction from the laser and specular directions. This feature could be caused by the formation of a strong static magnetic field along the target surface which traps and holds fast electrons on the surface. In our experiment, the increase in the laser intensity due to relativistic self-focusing in plasma plays an important role for the formation. The strength of the magnetic field is calculated from the bent angle of the electrons, resulting in tens of percent of laser magnetic field, which agrees well with a two-dimensional particle-in-cell calculation. The strong surface current explains the high conversion efficiency on the cone-guided fast ignitor experiments.

Recent progress in high power laser technologies allows us to study new regimes of laser-matter interactions relevant to astrophysics [1] and nuclear physics [2]. In the context of inertial fusion research, the ''fast ignitor'' [3] was proposed in order to relax the strict symmetry requirements for the laser irradiation of the spherical target and to reduce the drive energy needed to achieve high densities and the formation of the spark. However, the temporal and spatial stability is severely need to improve the propagation of the additional heating source, for example, because of losses and deflection of the ultraintense laser pulse in the surrounding plasma [4] and electron transport through the considerable length of a plasma [5].

An ''advanced fast ignitor'' is demonstrated for the purpose of gaining easy access to the fuel core using a solid guide for intense laser light [6]. In recent successful experiments using a gold cone shell target [7], a high energy coupling (20%–30%) from laser energy to compressed core was achieved. This efficiency is considerably higher than the expectation from the hot electron temperature in planar target experiments considering a classical stopping range of fast electrons at the fuel core. Anomalous stopping of fast electrons due to a strong electrostatic field induced by fast electrons themselves is a likely candidate of high efficiency core heating [8], and a full-scale particle-in-cell (PIC) simulation shows 35% energy coupling due to the anomalous stopping process [9].

In a recent paper another possibility is shown by the detailed analysis using a three-dimensional PIC simulation [10]. The result indicates that lower energy fast electrons flow along the inner cone walls and finally concentrate on the cone tip, which in turn heats the core effectively, although higher energy electrons penetrate the cone wall. However, it contradicts recent experimental results using a planar target with oblique laser incidence which show that the fast electrons are accelerated to laser direction by $J \times B$ heating [11] or target normal direction by resonant and

Brunel processes [12] according to plasma and laser conditions [13]. From this point of view, we have studied laser-plasma interactions with shallow incident angles to investigate the detail of the interaction mechanism between laser light and cone wall.

The experiments were performed using the GMII 30TW laser system at Osaka University [14]. The 1 μm intense laser light (20 J/600 fs) irradiates a 20 μm Al target at a shallow incident angle, typically 60° from the normal. Preformed plasma can be created before arriving at the main pulse using a separate beam line with long pulse duration (1 J/300 ps). The timing of the main pulse is fixed at the peak of the long pulse through the experiment. The size of preformed plasma was observed using a laser probe beam with an optical interferometer at the short pulse irradiation.

The emission angle of the fast electrons was measured with a stack of imaging plates (IPs) (FUJI Film, BAS-SR2025), which is well calibrated over a wide range of electron energies [15]. The stack consists of 4 IP layers and several filters including Al (12 μm), plastic (500 μm), and acryle (5 mm $\times$ 3 layers between each IP layers) against ions and x rays as well as ω_0 and $2\omega_0$ emissions. The stack was located 10 mm behind the target. To cover the wide range of the electron emission direction, the size of the IPs (H63 mm $\times$ W38 mm) is considerably larger than target size, which is a 500 μm square. The signal position on the IPs is converted into angles to the target normal; i.e., the vertical angle is for the tilting direction of the target.

Figure 1 shows a spatial distribution of electron emission taken when no plasma is presented at the laser intensity of 3×10^{18} W/cm^2. The horizontal dashed lines in the figure represent the electron emission angle to laser axis, target surface, and specular and target normal directions, from top to bottom. The vertical line profile is added at the side of the image to identify the peak position. The electrons are clearly emitted at the laser axis and also outside of
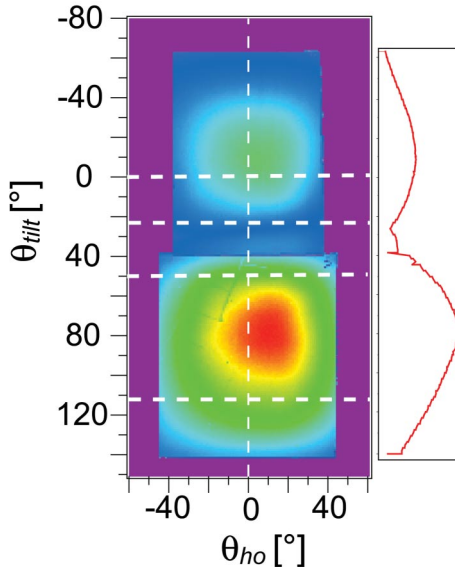
FIG. 1 (color).   Spatial electron distribution for the no plasma case. The horizontal lines represent angles for laser axis, target surface, and specular and target normal directions from top to bottom.

the specular direction. This outside specular emission is same direction as so-called ''specular jet'' observed in the several previous works [16].

On the other hand, as a plasma exists, the electron emission shows remarkable changes with the laser intensity. Figures 2(a)–2(c) indicate the emission direction taken at 1×10^{17}, 1×10^{18}, and 3×10^{18} W/cm^2 of laser intensity, respectively. In these panels, the three horizontal dashed lines indicate the laser axis, target surface, and specular directions, respectively. At the lower intensity [Fig. 2(a)], the emission direction is the same as the direction without plasma case. However, as laser intensity increases, the emission becomes close to target surface direction. In particular, at highest intensity shot [Fig. 2(c)], the emission angle is completely on the target surface direction.

This surface electron acceleration mechanism has been already indicated by the PIC calculations [10,17]. In the beginning, the strong magnetic field is generated due to the discontinuity of the laser field according to the Maxwell equation [$B(z) = \partial A(z)/\partial z$] at the critical surface. When

the laser incident angle is sufficiently large, the fast electrons are trapped by the magnetic field and then flow along the target surface. This surface current and its return current enhance the surface magnetic field. Such positive feedback holds the strong surface current during the laser irradiation.

In order to confirm this possibility, we performed two-dimensional PIC simulations with several laser and plasma conditions. Figure 3 shows the calculated two-dimensional electron momentum distributions. The gray rectangle on the right side of each picture represents an initial plasma region, and an intense laser irradiates at 60° incidence (yellow arrow) on it. The two white dashed lines show the laser incidence (right) and specular (left) directions. At a near solid plasma condition (scale length $L = 0.1$ μm) with the laser intensity $I = 10^{18}$ W/cm^2, the electron emission direction is strongly collimated toward the target surface direction, as well as a small fraction to the laser direction as shown in Fig. 3(a). However, when even a thin plasma exists ($L = 0.5$ μm), the electron acceleration directions are completely changed to the specular jet direction and almost no surface current can be observed [Fig. 3(b)]. On the other hand, when the laser intensity increase to 10^{19} W/cm^2, the PIC calculation shows that the fast electron emission is recovered to the surface direction even in the existence of small plasma ($L = 0.5$ μm), as shown in Fig. 3(c). These calculations indicate that the sufficient strength of the laser field is important to create the surface current depending on the plasma scale length.

The scale length dependence in the PIC calculations at the lower intensity case appears inconsistent with the experimental results. In addition, the electron emission parallel to the surface direction has been observed experimentally even at slightly lower intensity compared with the calculation. Here, comparing Figs. 1 and 2(c), the emission cone angle of electrons to laser direction for the no plasma case is clearly larger than that with the plasma condition (<25° and >45° with and without plasma case). This fact, the reduction of the electron emission cone angle may imply relativistic self-focusing in plasma [18,19] because the resulting higher intensity laser could transfer their moment onto the electrons more effectively to its direction.

We have performed a two-dimensional ray-trace calculation to estimate the increase of laser intensity via relativistic self-focusing using a realistic plasma density taken
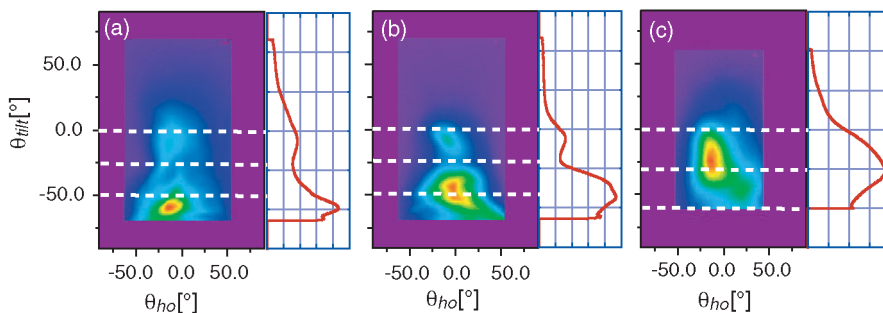

FIG. 2 (color).   Intensity dependence of electron emission angle with plasma condition at (a) 1×10^{17}, (b) 1×10^{18}, and (c) 3×10^{18} W/cm^2, respectively. The horizontal lines represent the laser axis, target surface, and specular directions from top to bottom. Because of a few percent of target setting accuracy, the incident angles of each shot were (a) 66°, (b) 64°, and (c) 59°.
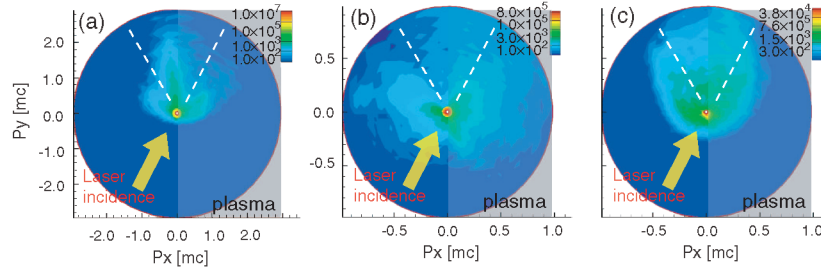
FIG. 3 (color).   Electron momentum distribution changing laser intensity for (a) laser intensity $I = 10^{18}$ W/cm^2 and initial plasma scale length at critical $L = 0.1$ μm, (b) $I = 10^{18}$ W/cm^2 and $L = 0.5$ μm, and (c) $I = 10^{19}$ W/cm^2 and $L = 0.5$ μm. The plasma position is covered by gray box, and the laser incidence is represented by yellow arrow in both figures.

from the interferometer images. At the start of the calculation, a Gaussian profile beam is located at 90 μm back from the target position, where the spot size becomes comparable to 20 μm in our focusing system, with a 60° incident angle in the simulation box. The calculation stops when the laser reaches at the relativistic critical density. As a result, at the lower intensity case (1×10^{18} W/cm^2), self-focusing does not occur because the power could barely reach the critical power of relativistic self-focusing ($P_c = 17.4(n_c/n_e)$ [GW]). On the other hand, at higher intensity case (3×10^{18} W/cm^2), the laser intensity significantly increases to 10^{19} W/cm^2 as shown in Table I. Such higher intensity laser light can reach 2 times the critical density due to the relativistic transparency [20], where the scale length is less than 1 μm, whereas the scale length at classical critical density is expected to be 3–4 μm. For such increased laser intensity and shortened scale length conditions, surface current formation is sufficiently possible at the high intensity case.

Figure 4 shows a series of electron emission distributions on each IP layer for (a) the low intensity case (10^{17} W/cm^2) and (b) the high intensity case (3×10^{18} W/cm^2). The minimum detectable electron energies are (i) 550 keV, (ii) 1.9 MeV, (iii) 3.0 MeV, and (iv) 4.2 MeV for the laser incidence direction (above the target surface direction in the image) and (i) 400 keV, (ii) 1.7 MeV, (iii) 2.9 MeV, and (iv) 4.2 MeV for the specular direction (below the surface direction). The horizontal dashed lines also represent laser incidence, target surface, and specular directions, from top to bottom. The color in each image is normalized with its peak signal. At the lower intensity case, the electron emission direction toward laser incidence is almost same for various energy electrons. For the specular direction, the emission angle becomes close to the exact specular direction from the first

to the second image, and then seems to be constant over the fourth image. This shift corresponds to matching of the momentum transition from laser light to higher energy electrons [21]. On the other hand, at the higher intensity case, the emission direction is widely ranging from laser incidence to surface direction on the second layer, even for the peak on the surface direction. In the deeper layers, both the peak position and emission range shift toward the laser axis. This feature, the higher energy electrons tending to accelerated toward laser axis, clearly indicates that escaping of higher energy electrons [10] and the possibility of bending by the surface magnetic field.

The surface magnetic field can be calculated from the bent angle of fast electrons. Assuming a Maxwellian as an electron energy distribution, the electron temperature is obtained from the least square fitting using the signal peak intensities and the average electron energy for each layer, $\bar{E} = \int_{E_{DL}}^{\infty} E f(E) dE / \int_{E_{DL}}^{\infty} f(E) dE$, where E_{DL} is the
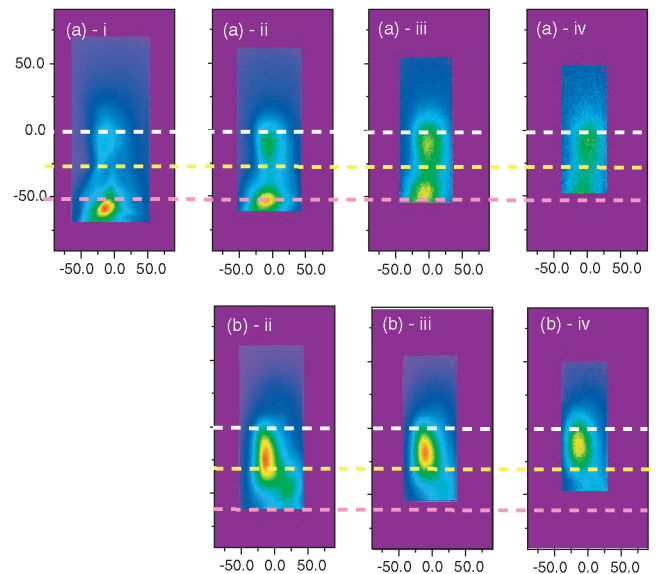

FIG. 4 (color).   Electron emission distribution on each IP layer for (a) the low intensity case (10^{17} W/cm^2) and (b) the high intensity case (3×10^{18} W/cm^2). The horizontal lines represent the laser axis, target surface, and specular directions from top to bottom. The color on each image is normalized by its peak signal.

TABLE I.   Increase of laser intensity due to relativistic self-focusing from a two-dimensional ray-trace calculation.

Initial intensity	Maximum intensity	Relativistic n_e
3×10^{18}	9.85×10^{18}	$2.1 \times n_c$
1×10^{18}	1.47×10^{18}	$1.2 \times n_c$

detection limit energy, resulting in 1.49 MeV at higher intensity case. On the other hand, the electron energies were 1.19 and 0.85 MeV for the laser and the specular direction when the laser intensity was 10^{17} W/cm^2. Using these average energies and assuming the electron acceleration direction to laser axis, the strength of magnetic field is order of a few tens of MG/z [μm], where z represents the depth of surface magnetic field. Assuming the depth between 100 nm (skin depth from the PIC calculation) and 1 μm (scale length), the magnetic field becomes about a few tens of percent of laser magnetic field when laser intensity is 10^{19} W/cm^2 and is comparable to the PIC prediction [17].

One can imagine a competing effect to bend the electron direction by the electrostatic field at the target rear side. It is well known that the strong static field, created between escaping electrons and target ions, accelerates ions to the MeV energy level toward the target normal direction [22]. The static field, $E \simeq \sqrt{2}kT_H/el_D$, where T_H is the electron temperature and l_D the Debye length, becomes the order of 10^{12} V/m in our experimental conditions. However, we conclude that the electrostatic field is implausible to bend the electrons because (i) the strength of the static field required to distort the electron emission direction is only of order 10^{10} V/m and (ii) it is extremely difficult to explain the change of emission angle with and without plasma conditions. Recent works indicate that no electron comes away due to refluxing and recirculating of fast electrons by a strong static field at the target rear side after initial electrons pass through to the target [23]. This effect suggests the electrons return back to the target before being bent by the static field. In our case, the formation time of static field can be delayed because of the decrease of fast electron current passing through the rear side when the surface current is formed. Note that a PIC shows refluxing of electrons becomes significant when a target thickness is less than half the laser duration (times light speed) such as in our case [24]. From these considerations, the surface magnetic field is most likely to be created when the laser intensity is sufficiently high according to the plasma scale length. In our case, these conditions could be achieved by increase of laser intensity due to relativistic self-focusing.

In summary, we observed spatial distributions of fast electrons emitted in intense laser-plasma interactions. The emission angle is changed from the specular direction to the target surface direction when preformed plasma is presented in front of the solid target. In addition, the emission angle also becomes close to the target surface with an increase of laser intensity. This change could be explained by the formation of a strong static magnetic field along the target surface due to trapping of fast electron at the surface. The relativistic self-focusing in our plasma condition gives the higher laser magnetic field which is significantly required for the surface current formation. The strength of the magnetic field is calculated from the bending angle of the emitted electrons detected at each layer of the detector, resulting in a few tens of percent of laser magnetic field. Such strong electron current along with the surface might bring the high conversion efficiency to the cone-guided fast ignitor experiments.

[*]Current address: Tata Institute of Fundamental Research, Colaba, Mumbai 400 005, India.

[†]Current address: Center for Ultrafast Optical Science, University of Michigan, 1006 Gerstacler, Ann Arbor, MI 48109, USA.

[1] B. A. Remington, D. Arnet, R. P. Drake, and H. Takabe, Science **284**, 1488 (1999).

[2] E. P. Liang, S. C. Wilks, and M. Tabak, Phys. Rev. Lett. **81**, 4887 (1998).

[3] M. Tabak *et al.*, Phys. Plasmas **1**, 1626 (1994).

[4] B. J. Duda, R. G. Hemker, K. C. Tzeng, and W. B. Mori, Phys. Rev. Lett. **83**, 1978 (1999).

[5] S. Hain, F. Cornolti, and H. Opower, Laser Part. Beams **17**, 245 (1999).

[6] P. A. Norreys *et al.*, Phys. Plasmas **7**, 3721 (2000).

[7] R. Kodama *et al.*, Nature (London) **412**, 798 (2001); **418**, 933 (2002).

[8] Y. Sentoku, K. Mima, P. Kaw, and K. Nishikawa, Phys. Rev. Lett. **90**, 155001 (2003).

[9] R. B. Campbell, R. Kodama, T. A. Mehlhorn, K. A. Tanaka, and D. R. Welch, Phys. Rev. Lett. **94**, 055001 (2005).

[10] Y. Sentoku, K. Mima, H. Ruhl, Y. Toyama, R. Kodama, and T. E. Cowan, Phys. Plasmas **11**, 3083 (2004).

[11] S. C. Wilks, W. L. Kruer, M. Tabak, and A. B. Langdon, Phys. Rev. Lett. **69**, 1383 (1992).

[12] F. Brunel, Phys. Rev. Lett. **59**, 52 (1987).

[13] M. I. K. Santala *et al.*, Phys. Rev. Lett. **84**, 1459 (2000).

[14] Y. Kitagawa *et al.*, Fusion Eng. Des. **44**, 261 (1999).

[15] K. A. Tanaka, T. Yabuuchi, T. Sato, R. Kodama, Y. Kitagawa, T. Ikeda, Y. Honda, and S. Okuda, Rev. Sci. Instrum. **76**, 013507 (2005).

[16] R. Kodama, K. A. Tanaka, Y. Sentoku, T. Matsushita, K. Takahashi, H. Fujita, Y. Kitagawa, Y. Kato, T. Yamanaka, and K. Mima, Phys. Rev. Lett. **84**, 674 (2000).

[17] T. Nakamura, S. Kato, H. Nagatomo, and K. Mima, Phys. Rev. Lett. **93**, 265002 (2004).

[18] C. Gahn *et al.*, Phys. Plasmas **9**, 987 (2002).

[19] Y. T. Li *et al.*, Phys. Rev. E **69**, 036405 (2004).

[20] E. Lefebvre and G. Bonnaud, Phys. Rev. Lett. **74**, 2002 (1995).

[21] H. Ruhl, Y. Sentoku, K. Mima, K. A. Tanaka, and R. Kodama, Phys. Rev. Lett. **82**, 743 (1999).

[22] S. P. Hatchett *et al.*, Phys. Plasmas **7**, 2076 (2000); R. A. Snavely *et al.*, Phys. Rev. Lett. **85**, 2945 (2000).

[23] A. J. Mackinnon *et al.*, Phys. Rev. Lett. **88**, 215006 (2002).

[24] Y. Sentoku *et al.*, Phys. Plasmas **10**, 2009 (2003).